Vegetation-Droplet Effects on Canopy Interception and Ground Deposition in Aerial Application of Fire-extinguishing Agent

Sheng-Hua Xiong
Civil Aviation Flight University of China
Yan-Zhao Shi
Civil Aviation Flight University of China
Wan-Ki Chow
Hong Kong Polytechnic University
Yuan-Hua He
heyuanhua@cafuc.edu.cn

Civil Aviation Flight University of China

Research Article

Keywords: Aerial application of fire-extinguishing agent, Canopy interception, Ground deposition, Relative importance analysis

Posted Date: November 28th, 2025

DOI: https://doi.org/10.21203/rs.3.rs-8145969/v1

Additional Declarations: No competing interests reported.

Vegetation-Droplet Effects on Canopy Interception and Ground Deposition in Aerial Application of Fire-extinguishing Agent

Abstract: Aerial application of fire-extinguishing agent is an important method for rapidly constructing firebreaks. Using spray experiments on *Schima superba* and *Pinus massoniana*, this study examines how vegetation and droplet properties affect canopy interception and ground deposition during canopy penetration. Droplet velocity and size distributions were measured using particle image velocimetry and image analysis, and leaf hydrophobicity was measured by contact-angle goniometry. Subsequently, based on fire-extinguishing agent spray experiments and a relative importance analysis, the influences of vegetation and droplet properties on canopy interception and ground deposition were quantified. The results show that the static contact angle of *Pinus massoniana* is 14.5% higher than *Schima superba*. Moreover, compared with *Schima superba*, *Pinus massoniana* exhibits higher interception and lagged-dripping capacities, and this trend becomes more pronounced as LAI increases. When LAI rises from 1.2 to 2.18, the interception-rate difference between *Pinus massoniana* and *Schima superba* increases from 1.2% to 2.8%, while the difference in lagged dripping increases from 9.8% to 11.2%. Finally, according to the relative-importance results, the average contributions of flow rate, droplet size, and velocity to interception and deposition are 49.28%/46.95%, 40.77%/41.92%, and 10.82%/11.13%, respectively, yielding a consistent ranking of influence: *flow rate>droplet size>velocity*.

Keywords: Aerial application of fire-extinguishing agent; Canopy interception; Ground deposition; Relative importance analysis

1. Introduction

Southwest China is characterized by pronounced topographic relief, extensive montane forests, high forest cover, and a complex mosaic of vegetation types. Under the combined influences of hot, dry weather, frequent thunderstorms, agricultural burning, and topography-induced ventilation, this region constitutes one of the highest-risk areas for forest fires in China (Zhao, J et al. 2022). In complex firegrounds, differentiated suppression strategies are required for distinct zones. Along the fireline, operations typically prioritize rapid knockdown, often employing high-pressure water or constructing handlines to curb spread. In high-temperature core zones, cooling and pressure relief measures are adopted to prevent re-ignition. In peripheral areas, the focus shifts to building firebreaks to halt outward spread and avoid the formation of a secondary fire front (Tezcan 2025). Among diverse suppression methods, constructing firebreaks, by severing fuel continuity, interrupting fire transmission, and providing time for subsequent operations, is widely regarded as a critical component of large-scale forest fire prevention and control. Consequently, constructing firebreaks both efficiently and safely has emerged as a key research priority for enhancing forest fire prevention and control capacity.

Firebreak construction primarily encompasses physical isolation and aerial extinguishing agent application. Physical isolation entails the manual establishment of breaks under suitable fireground conditions to interrupt fuel continuity and thereby impedes fire propagation (Cui et al. 2019, Ingalsbee 2005). Aerial application involves delivering fire-extinguishing agent from aircraft, enabling droplet deposition and adhesion to vegetation surfaces to form a continuous film that mechanistically suppresses combustion reactions and heat transfer, thereby establishing a fire-extinguishing agent firebreak (Gaikwad et al. 2024). Compared with physical methods, aerial delivery offers adaptability for remote deployment in complex terrain, thus conferring significant strategic value in enhancing suppression efficiency and operational safety. In wildfire-prone countries worldwide, aerial firefighting systems have become increasingly mature and are often deployed as integrated, multi-tiered systems. For large aircraft and heavy firefighting helicopters, exemplified by the DC-10 and C-130 in the United States and Canada, and China's domestically developed AG600 large amphibious aircraft, long-range, high-volume drops enable the rapid construction of firebreaks and fire-line containment (Struminska and Filippone 2024, Yang 2024). Meanwhile, the expanding use of multi-type UAV platforms and small fixed-wing aircraft for wildfire sensing, precision applications, and intelligent path planning is driving aerial firefighting toward greater diversification, automation, and data-driven decision-making (Lu 2023, Lattimer 2023).

The aircraft's flight altitude, airspeed, and spray tank design are factors that influence droplet ejection velocity, size distribution, and spatial coverage. The complete spray-transport pathway from a fluid mechanics perspective, linking six stages: liquid ejection, jet penetration, jet breakup, surface atomization, droplet descent, and canopy traversal through vegetation (Dominique 2024). PIV and image analysis were used to analyze water release from firefighting drop aircraft under various operating conditions, revealing that release parameters strongly affect the multiscale breakup mechanisms and macroscopic dispersion patterns of the water. (Ito et al. 2010). An Eulerian approach was employed to model the water-drop process of the AG600, quantifying the effects of aircraft speed, drop volume, and release altitude on droplet dynamics and coverage (Tian et al. 2019). In 2022, how initial velocity, droplet size, and ejection direction influenced the trajectory and reach of liquid-nitrogen suppressant droplets (Liu 2022). The three-dimensional model was built based on the M18BDromader aircraft and investigated how flight speed, altitude, and release position affect the areal extent and density of the droplet field (Czyż et al. 2023), and a Bell 206L-4 helicopter platform was used to investigate the droplet size distributions of three flat-fan nozzles under low-to-moderate wind-tunnel conditions and during field flights (Yao et al. 2020). Changes in nozzle design and system pressurization levels were systematically examined in terms of their effects on ejection velocity, spray angle, overall dispersion efficiency of the suppressant, and the downwash airflow velocity field generated by a single-rotor UAV during operation. (Shrigondekar et al. 2021 Zhang et al. 2024). Downwash directly beneath the airframe is approximately vertical and downward, weakens progressively with increasing height, and spreads outward in the near-ground layer. These characteristics provide experimental evidence for the motion of suppressant droplets under airflow conditions (Wang et al. 2023).

The final stage, where droplets penetrate the vegetation canopy and deposit on the ground, is critical to the fire-prevention and containment effectiveness of the fire-extinguishing agent. Droplet deposition capacity is significantly influenced by factors such as vegetation cover, leaf traits, droplet velocity, size, and flow rate across different delivery methods. Through single-leaf dynamic contact angle experiments, differing surface properties among plant leaves lead to significant differences in adhesion (Ma et al. 2022). Based on contact-angle and surface-tension measurements, a larger contact angle indicates poorer wettability of the coal surface (Wang et al.2023). The impact and behavior of spray droplets on horizontal hydrophobic surfaces were investigated, revealing the synergistic roles of droplet kinetic energy and surface wettability in governing adhesion, rebound, and breakup (Zwertvaegher et al. 2014). High-speed imaging was combined with numerical simulations to examine the reverse-jet behavior of different hollow droplets under varying impact velocities and synthetic superhydrophobic surfaces (Nahdi et al. 2021, Kuznetsov et al. 2021). Considering the influence of vegetation traits on droplet deposition (Loudermilk et al. 2022). Based on field observations of three forest types in Shanxi Province and simulations with a vegetation-interception model, canopy interception capacity was found to decrease in the order: *broadleaf mixed forest > broadleaf forest > evergreen forest* (Zhou et al.2025). The Gauss-Newton algorithm was used to optimize parameters of a leaf-surface deposition model, integrated vegetation structural indicators to analyze droplet interception, and developed an interception prediction model adaptable to the canopy structures of different tree species (Yi et al. 2025). Based on field observations comparing four representative tree species in the Pacific region, found that coniferous forests maintain a high canopy deposition and interception rate in both the dormant and growing seasons. In contrast, broadleaf species exhibit stronger interception primarily during leaf-out (Fischer et al. 2023). The LAI has a significant effect on rainfall interception in Qinghai spruce forests. At high elevations, a higher LAI enables more effective precipitation interception, yielding higher canopy interception rates. In contrast, at low elevations, a lower LAI reduces the interception rate by 3.3% relative to high elevations. (Yang et al. 2024). A model was developed for droplet deposition of an AF-25B helicopter at different flight altitudes. They found that flying at a lower altitude increases the outward spread of airflow but results in less uniform droplet distribution; conversely, raising the altitude improves spray uniformity but markedly reduces deposition efficiency (Tang et al. 2020). A method for modeling tree-crown morphology was proposed, and extinguishing agent deposition at different heights during canopy penetration was quantitatively analyzed, thereby elucidating the dynamic mechanisms of canopy droplet deposition. (Calogine et al. 2007). The spraying tests under various UAV operating parameters showed that smaller droplets have lower deposition efficiency, whereas larger droplets adhere more readily to vegetation and experience significantly less drift (Shan et al. 2024). Interception by typical vegetation under different rainfall intensities, for individual shrubs, interception increases from low to moderate intensities but declines at high intensities because of stronger raindrop impact and enhanced splash (Wang et al. 2018, Silva et al. 2024). The three-dimensional simulations and a particle swarm optimization algorithm were used to analyze droplet deposition efficiency across flight altitudes and speeds, and derived an optimal parameter combination that significantly improves deposition rates (Xu et al. 2023). Bench-scale controlled combustion experiments were employed to evaluate the effects of extinguishing agent concentration and other physical parameters on the fire-resistance performance of wildland pine-needle fuels (Álvarez et al. 2025).

In aerial fire-extinguishing agent operations, droplet interception and deposition during traversal of complex vegetation canopies are governed not only by flight parameters but also by vegetation structure and type. Prior studies have shown that aircraft airspeed, release altitude, and tank design markedly influence droplet formation and initial conditions. However, during canopy traversal, the specific mechanisms by which different vegetation types influence droplet interception and deposition, and the relative importance of drop parameters in modulating these processes, are not yet well quantified and systematically assessed. To address this gap, this study developed a nozzle-based spray platform to simulate the physical processes of fire-extinguishing agent droplet penetration of the canopy and deposition on the ground during aerial application.

The main contributions of this study are as follows:

(1) Characterization of the velocity and droplet size distribution of nozzle-released fire-extinguishing agent using Particle Image Velocimetry (PIV) and droplet sizing algorithms to establish the physical spray parameters during the canopy-penetration stage of aerial application.

(2) Quantification of the hydrophobicity differences between *Schima superba* and *Pinus massoniana* leaves using a contact angle goniometer to provide a basis for interpreting how droplet properties influence canopy penetration behavior.

(3) Integration of the contact angle findings with fire-extinguishing agent spray test data to analyze how vegetation structure type, leaf area index, and spray factors affect fire-extinguishing agent canopy-penetration behavior.

(4) Application of multivariate linear regression and relative importance decomposition to evaluate the relative contributions of velocity, droplet size, and flow rate to canopy interception and ground deposition, and identify the most influential factor in canopy penetration.

The structure of this article is as follows: Section 2 introduces the selected vegetation types and details the experimental design and data analysis methods for three sub-experiments. Section 3, based on the experimental results established in Section 2, presents a systematic analysis of fire-extinguishing agent interception and deposition under various drop conditions and vegetation structures. It then discusses the study's practical implications and limitations. Section 4 summarizes the main conclusions.

2. Materials & Methods

2.1. Selection of Experimental Vegetation

This study selected two representative species commonly found in Southwest China as test subjects: the broadleaf tree *Schima superba* and the widely distributed conifer *Pinus massoniana* (chen et al. 2023). To eliminate the confounding effect of varying canopy cover, Leaf Area Index (LAI) was used as an index of canopy density (Wolter et al. 2021). An LAI meter (IN-G10, Laiyin Optoelectronics Technology Co., Shandong, China) was used to ensure consistency in LAI . Initial mass was measured using an electronic balance. Canopy height was recorded using a tape measure. Vegetation parameters were summarized in Table 1.

Table 1: Vegetation parameters

Vegetation type	Vegetation species	Height(m)	Crown breadth(m)	Canopy thickness (m)	Initial weight (g)	LAI	Number of branches
1	*Schima superba*	0.92	0.83×0.92	0.60	685.8	1.18	7
2	*Schima superba*	0.90	0.93×0.98	0.62	1072.9	2.15	11
3	*Pinus massoniana*	0.87	0.85×0.89	0.68	702.4	1.10	5
4	*Pinus massoniana*	0.91	0.92×1.02	0.65	1103.6	2.11	10

2.2. Experimental Design

This study comprises three experiments: Experiment (1) characterized the spray parameters, Experiment (2) investigated leaf surface properties (hydrophobicity), and Experiment (3) measured canopy interception and ground deposition. The experimental workflow diagram is presented in Figure 1.

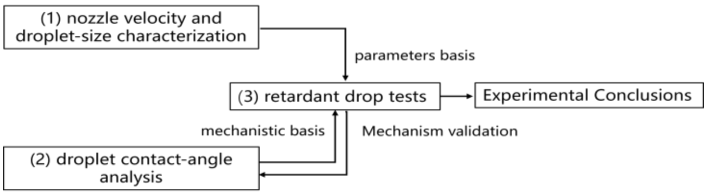

Figure 1 Experimental workflow diagram

2.2.1 Experimental Design for Droplet Velocity and Size Measurement

The droplet velocity field and droplet size distribution of the fire-extinguishing agent discharged from the nozzle were characterized by varying pump pressure and nozzle orifice diameter. The setup for measuring nozzle velocity and droplet size is shown in Figure 2

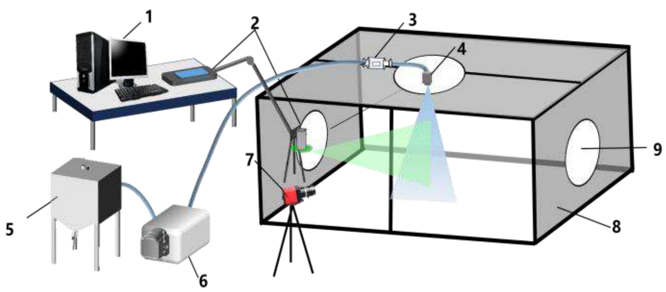

Figure 2 Schematic of the droplet velocity and size measurement setup
(1-Computer; 2-PIV system; 3-Flowmeter; 4-Nozzle assembly; 5-Water tank; 6-Pump unit; 7-High-speed camera; 8- High-strength glass chamber; 9-Viewing window)

In the experiments, the water-based fire-extinguishing agent (main components: 18% phosphorus compounds and 14% nitrogen compounds) was stored in a water tank and pressurized by a variable-pressure pump. To examine droplet velocity, a PIV system (RFlow-2D3C, Hefei Zhongke Junda Vision Technology Co., Anhui, China) was used to measure the two-dimensional velocity field of atomized droplets within a 10×10 *cm* field of view at the nozzle exit (Liu et al.2024, Widmann 2001). In parallel, droplet sequences recorded by a high-speed camera were analyzed for size distribution via grayscale processing, scale calibration, binarization, edge extraction, and circle fitting (Erinin et al. 2023). To systematically characterize the effect of nozzle orifice diameter and pump pressure coefficient, five nozzle sizes were configured to form a continuous spectrum ranging from "fine mist" to "medium" to "coarse". The characterization spray conditions are summarized in Table 2.

Table 2 Characterization spray conditions

Test Group	Nozzle Orifice Diameter(*mm*)	Nozzle Diameter(*mm*)	Pump Pressure (*Mpa*)	Flow rate (*L*/*min*)	Mass spray rate S_t (*g*/*s*)
1-1	0.18	10.08	45	0.19	3.5
2-1	1.6	10.16	5	1.35	24.8
2-2	1.6	10.16	27	2.10	38.5
2-3	1.6	10.16	45	2.62	48.0
3-1	2.4	10.28	5	2.63	48.2
3-2	2.4	10.28	17	3.60	66.0
3-3	2.4	10.28	45	4.61	84.5
4-1	3.2	10.34	5	3.91	71.7
4-2	3.2	10.34	20	6.02	110.4
4-3	3.2	10.34	40	7.05	129.3
5-1	4.6	10.38	13	6.86	125.8
5-2	4.6	10.38	19	8.37	153.5

2.2.2 Experimental Design for Droplet Contact Angle Analysis

To examine the contact angles of fire-extinguishing agent droplets on different vegetation surfaces, a contact-angle goniometer (CA500S, Guangdong Beidou Precision Instruments Co., Ltd., Guangdong, China) was employed to perform single-leaf tests on *Schima superba* and *Pinus massoniana*. The schematic of the setup is shown in Figure 3.

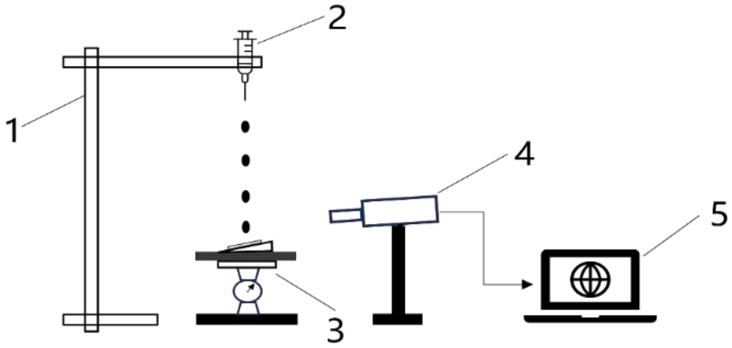

Figure 3 Schematic of the contact-angle measurement setup
(1-Fixed stand; 2-Microsyringe; 3-Stage; 4-High speed camera; 5-Computer)

An ellipse-fitting method was employed to determine contact angles. The droplet contour was fitted with an elliptical arc to automatically identify the intersection points between the droplet and the leaf surface [38]. To ensure reliability, tests were performed under identical conditions in triplicate.

2.2.3 Experimental Design for Fire-extinguishing Agent Spray Test

To investigate how different spray parameters and vegetation conditions affect fire-extinguishing agent interception and deposition, a spray apparatus was designed, as depicted in Figure 4, and the experimental design of the fire-extinguishing agent spray system is illustrated in Figure 5.

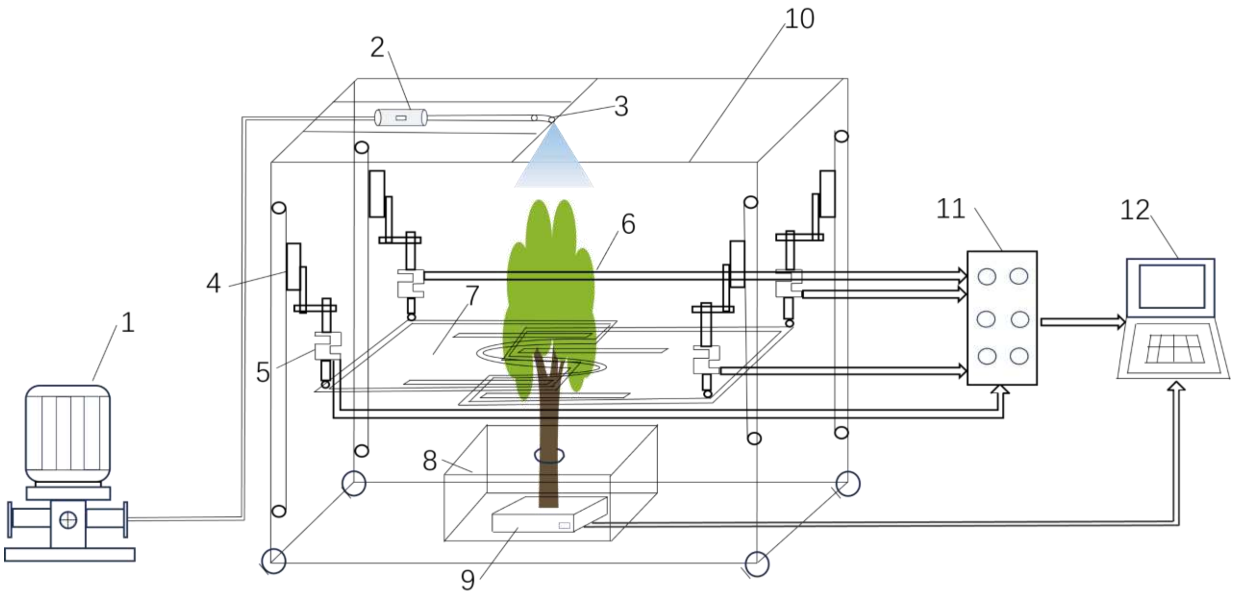

Figure 4 Schematic of the fire-extinguishing agent spray system
(1-Variable-frequency pump; 2-Flowmeter; 3-Atomizing nozzle; 4-Pulley assembly; 5-Tension sensor; 6-Vegetation; 7-Horizontal plate; 8-Rain shield; 9-Real time electronic balance; 10-Aluminum profile frame; 11-Communication converter; 12-Computer)

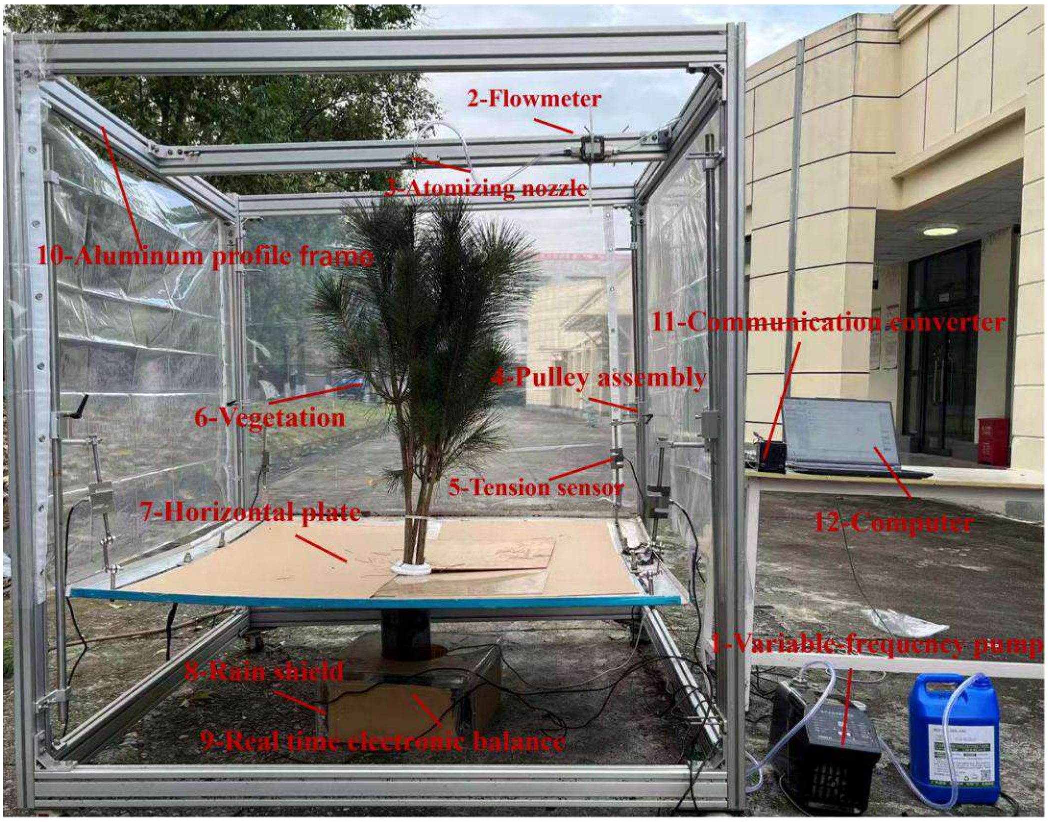

Figure 5 Experimental Design of the fire-extinguishing agent Spray System

Canopy interception and ground deposition were measured using a balance and tension load cells. Canopy interception was quantified using a real-time electronic balance (TSC-L, Shenzhen Feiya, Guangdong, China; 30*kg* capacity, 0.1*g* resolution, 1*s* sampling). Ground deposition was measured using a horizontal plate supported by four tension load cells (PBCL-03, Bengbu Dingli Electronic Technology Co., Ltd., Anhui, China; 50*kg* capacity, 0.1*g* resolution, 1*s* sampling). Signals from the four sensors were combined via a junction box and transmitted to the computer. To minimize interference from stray runoff, a two-layer splash-guard design was adopted. The horizontal plate formed the first barrier, and the second barrier was a cubic box with vertical sidewalls and a central opening, which effectively isolated the interception measurement from external flows during spraying.

Following spray initiation, canopy interception was logged in real-time at 1*s* intervals. Spraying was terminated once a steady interception regime was reached, defined as a per-step increment less than a prescribed relative threshold $(\Delta_I \leq 0.05 S_t)$ for five consecutive time steps. The interception at this point was recorded as the saturated interception $(I_{\max})$ (Ma et al. 2022). Concurrently, based on the deposition volume (D) corresponding to the saturated interception time, the spray volume (S) and spray duration were recorded (t). The saturated deposition fraction $(D_{rate} = D/S)$, the saturated interception fraction $(I_{rate} = I_{\max}/S)$, the interception volume per unit amount $(I_{\mathrm{t}} = I_{\max}/t)$, and deposition volume per unit time amount $(D_{\mathrm{t}} = D/t)$ were computed.

After spraying was completed, monitoring continued at 1s intervals. When the balance reading stabilized with fluctuations ≤1g over five consecutive time steps, the reading was considered the stabilized interception $(\mathrm{I}_{\min})$ (Wang et al.2018). The difference between the saturated and stabilized interception was defined as the lagged dripping volume (I_{fall}). After each experiment, vegetation was thoroughly rinsed and air-dried outdoors. The subsequent run commenced only after the initial plant mass had returned to within ±5% of its pre-test value, thereby ensuring consistency and repeatability. Each condition was tested in triplicate under identical conditions.

3. Experimental Results and Discussions

This section presents and discusses the results of the experimental program described in Section 2. The central objective is to elucidate how vegetation and droplet characteristics govern fire-extinguishing agent canopy interception and ground deposition.

3.1. Droplet Velocity and Size Characterization

Following the experimental design described in Section 2.2.1, velocity field contour maps of the fire-extinguishing agent under different spray conditions were presented in Figure 6.

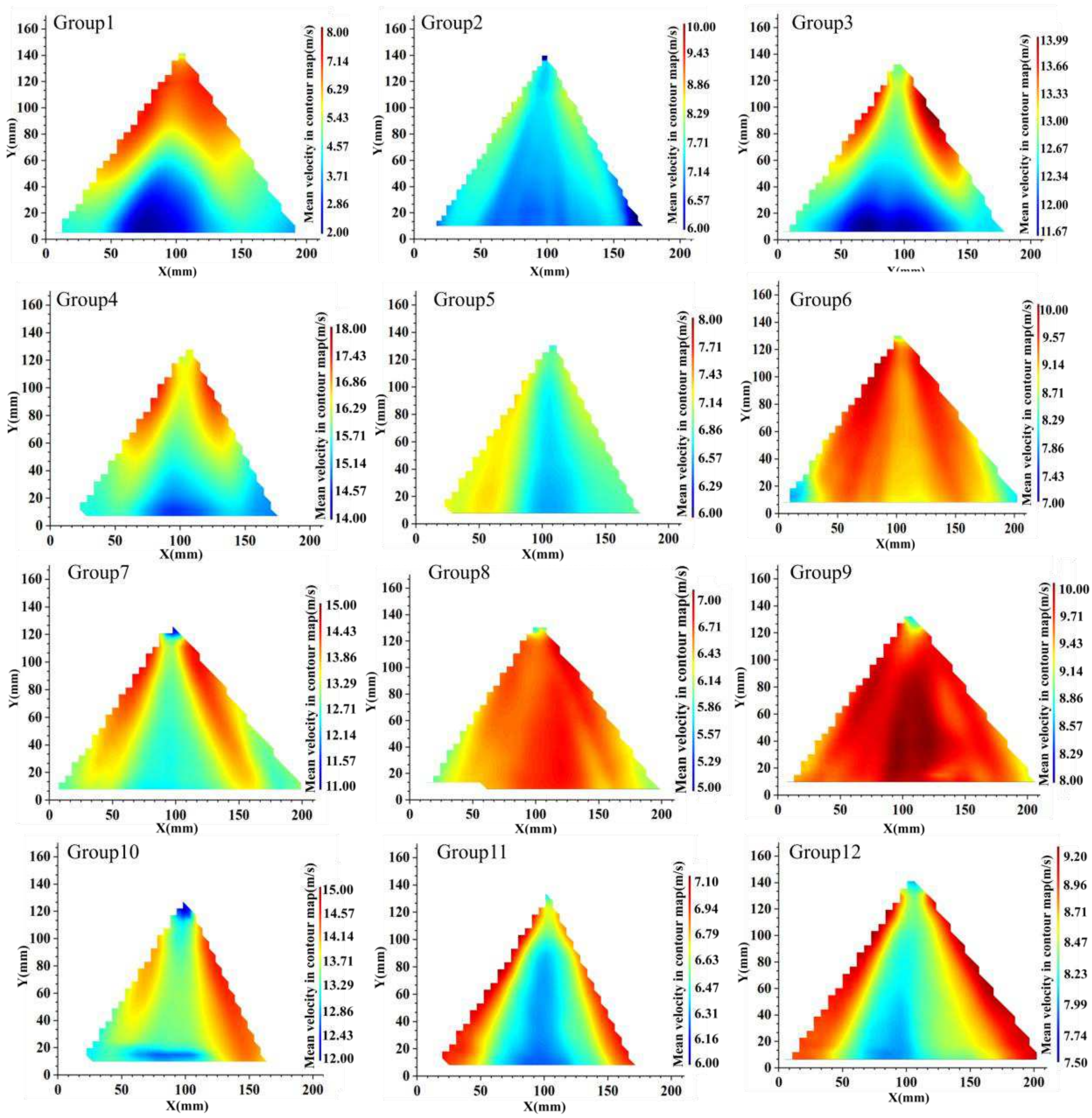

Figure 6 PIV velocity field contour map

From the PIV velocity contour maps in Figure 6, the droplet velocity field exhibits a profile with higher velocities at the lateral edges and lower velocities at the center. Under different combinations of nozzle and pump pressure settings, both droplet velocities and the effective field of view vary markedly; three independent replicates were summarized in Table 3. To determine droplet size distributions, high-speed and high-resolution images were analyzed using a shadowgraph approach for non-contact sizing of fragmented droplets. Raw images were first converted to grayscale to enhance droplet-background contrast, and the nozzle geometry served as the scale reference for pixel-to-length calibration, as illustrated in Figure 7(a).

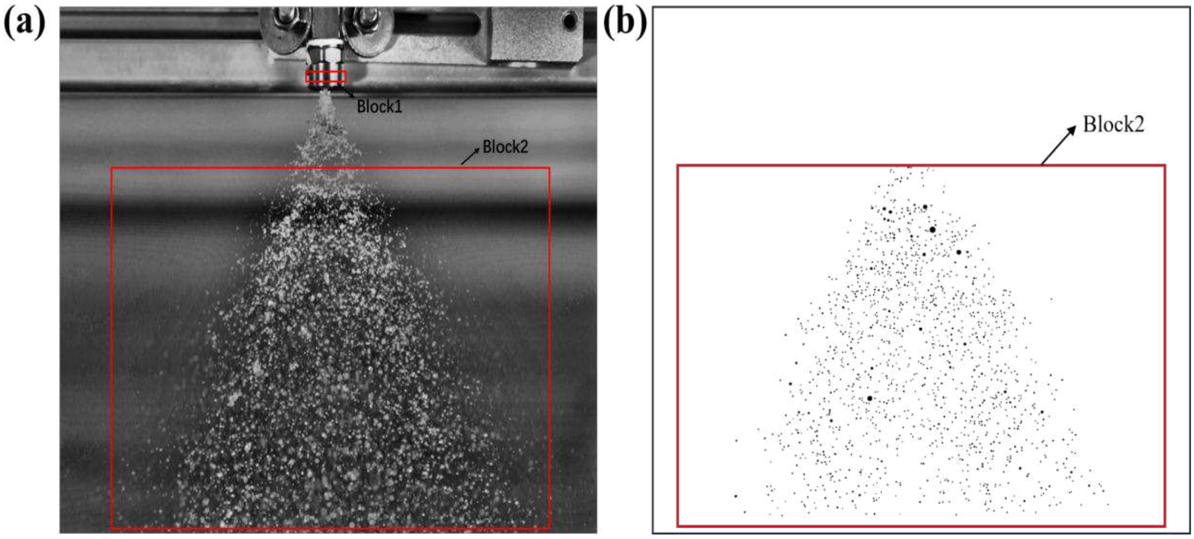

Figure 7 Droplet Image Processing Diagram
((a) Grayscale processing and image calibration schematic for fire-extinguishing agent droplets; (b) Contour extraction of fire-extinguishing agent droplets)

In Figure 8, Block 1 denoted the nozzle calibration region, and Block 2 denoted the droplet size calibration region. Using the known physical orifice diameter at the nozzle exit and its corresponding pixel span within the same frame, spatial calibration was performed to establish the pixel-to-physical scale relationship given by formula (3-1), thereby mapping the image scale to the actual droplet diameter.

$$S_{rate} = \frac{D_{real}}{W_{pixel}} \tag{3-1}$$

where D_{real} is the actual nozzle orifice diameter, W_{pixel} is the pixel span of the known orifice in the same frame, and S_{rate} is the pixel resolution corresponding to the extracted nozzle dimension in the image.

Following grayscale conversion and spatial calibration, the calibrated images were processed using adaptive thresholding and Canny edge detection to extract candidate droplet contours. To ensure measurement reliability, only candidate droplets that were sufficiently circular $\left(r \geq 0.85\right)$ and had pixel areas $A_k \geq 50px^2$ within the effective field of view were retained. The resulting droplet contours were shown in Figure 7(b). Based on the pixel area of each droplet and the calibrated scale, the area-equivalent diameter was computed using the equivalent circle model.

$$d_k = 2\times10^3 S_{rate}\sqrt{\frac{A_k}{\pi}} \quad (\mu m) \tag{3-2}$$

where d_k is the computed physical droplet diameter and S_{rate} is the pixel resolution obtained from formula (3-1). The computed diameters were summarized as a histogram, and the median diameter D_{50} was used as the evaluation metric. The droplet-size result for Group 2-1 is shown in Figure 8.

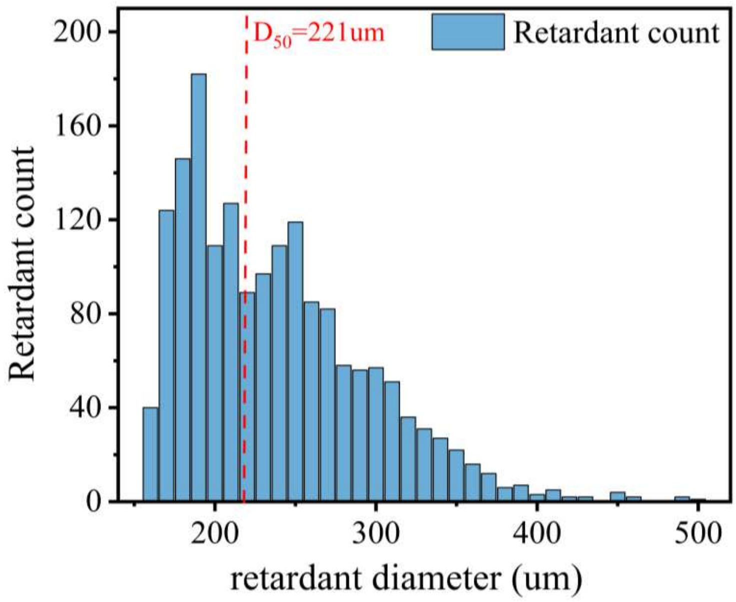

Figure 8 Droplet Size for Group 2-1

Similarly, for the remaining 11 groups listed in Table 2, the same image processing and droplet sizing workflow was applied: droplet contours were extracted and converted to physical diameters, yielding a size distribution for each condition for subsequent comparative analysis. To enhance robustness, three frames per condition, each containing no fewer than 500 valid droplets, were analyzed, and quality-controlled statistics were retained for further processing. Droplet velocity and size results are summarized in Table 3.

Table 3 fire-extinguishing agent droplet velocity and size results

Test group	Velocity (*m/s*)	D_{50} (μm)
1-1	3.42±0.12	93±14
2-1	6.80±0.18	216±12
2-2	13.00±0.07	202±16
2-3	15.20±0.09	191±14
3-1	6.95±0.15	278±9
3-2	9.12±0.13	255±13
3-3	13.24±0.07	247±11
4-1	6.27±0.13	355±12
4-2	9.74±0.16	347±15
4-3	13.82±0.13	332±10
5-1	6.74±0.08	385±16
5-2	8.41±0.15	376±12

According to Tables 2 and 3, the nozzle orifice diameter and the pump pressure control droplet velocity. At a fixed pump pressure, exit velocity decreased as orifice diameter increased; and at a fixed orifice diameter, exit velocity increased with pump pressure. Meanwhile , the droplet size reported as the median diameter was mainly influenced by orifice diameter and pump pressure. Specifically, the mist nozzle produced fine sprays with $D_{50} < 100\mu m$, whereas the larger-orifice nozzles yielded distributions concentrated between 200-400 μm. At the same time, higher pressure generally produces smaller droplets. Using Groups 2-1 to 2-3 as an example, the diameter in Group 2-3 was 11.5% lower than in Group 2-1 and 5.4% lower than in Group 2-2. Then, the exit velocity and droplet-size distributions will serve as the spray inputs for the subsequent spray experiments.

3.2. Leaf Hydrophobicity Analysis

The contact angle is a key metric for quantifying the hydrophobicity of droplets on leaf surfaces. The fire-extinguishing agent droplets deposited on the leaves of *Schima superba* and *Pinus massoniana* were analyzed, and the fitted results were shown in Figures 9 and 10. The results of the contact angle analysis were summarized in Table 4.

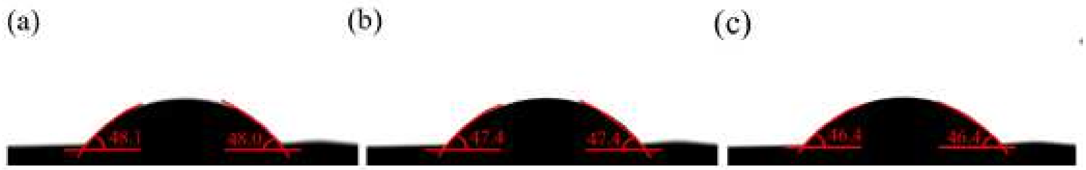

Figure 9 Static Contact Angle Measurement Results for *Schima superba* Leaves ((a) Test number 1; (b) Test number 2; (c) Test number 3)

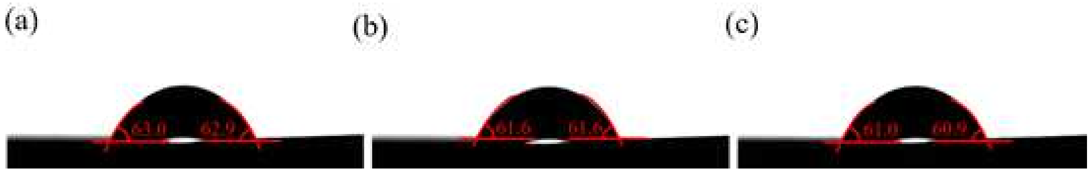

Figure 10 Static Contact Angle Measurement Results for *Pinus massoniana* Leaves ((a) Test number 4; (b) Test number 5; (c) Test number 6)

Table 4 Contact Angle Measurement Data

Test number	Vegetation species	droplet diameter (μm)	Left contact angle (°)	Right contact angle (°)	Mean contact angle (°)	Mean value(°)
1	*Schima superba*	3.751	48.092	48.080	48.086	
2	*Schima superba*	3.846	47.380	47.370	47.375	47.304± 0.83
3	*Schima superba*	4.519	46.440	46.436	46.438	
4	*Pinus massoniana*	3.154	62.951	62.944	62.948	
5	*Pinus massoniana*	3.453	61.579	61.559	61.564	61.85± 0.84°
6	*Pinus massoniana*	3.764	61.017	60.812	60.914	

Based on Figure 9, Figure 10 and Table 4, the static contact angle for *Pinus massoniana* leaves was significantly higher than that for *Schima superba* leaves. Furthermore, an increasing droplet size was associated with a reduction in the static contact angle. This indicates that, at the single-leaf scale, *Pinus massoniana* exhibits higher hydrophobicity and poorer droplet retention capacity than *Schima superba*.

3.3. Vegetation and Droplet Characteristics Effects on Interception and Deposition

Building upon the results presented in Section 3.1, this section details fire-extinguishing agent spray experiments conducted on the four vegetation types listed in Table 1. For *Schima* *superba*, canopy interception and ground deposition under two distinct LAI conditions are illustrated in Figure 11. The results for *Pinus massoniana* were presented in Figure 12. The corresponding experimental data were compiled in Tables 5-6 and Appendix A (Tables 10-11). Subsequently, this section compares the results using the evaluation metrics from Section 2.2.3 to elucidate how vegetation characteristics and droplet properties influence fire-extinguishing agent canopy interception and ground deposition.

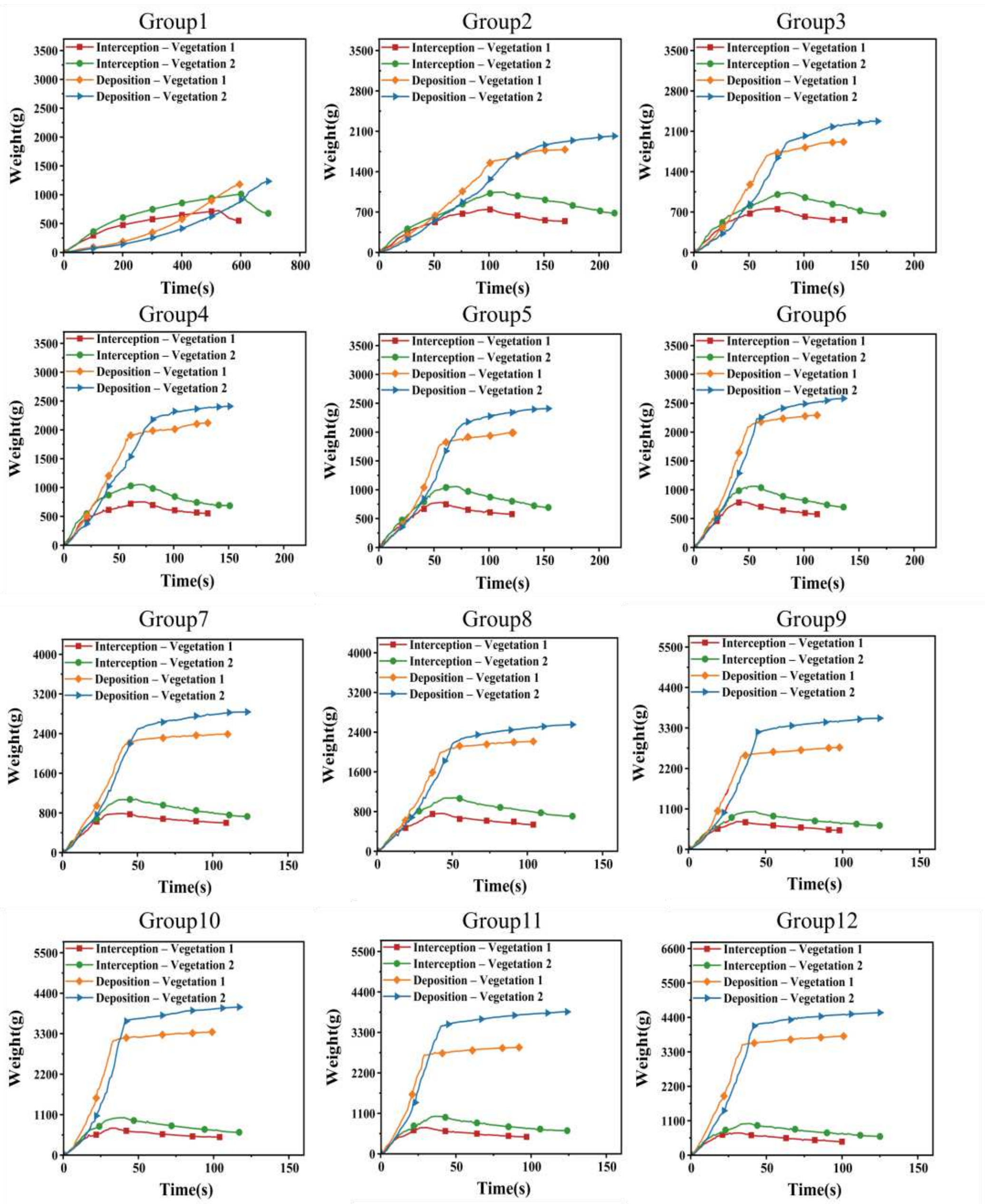

Figure 11 Experimental results for the fire-extinguishing agent canopy interception and ground deposition of *Schima superba* under different drop conditions

Figures 12 illustrate the trends in fire-extinguishing agent canopy interception and ground deposition for *Pinus massoniana* under various spray conditions.

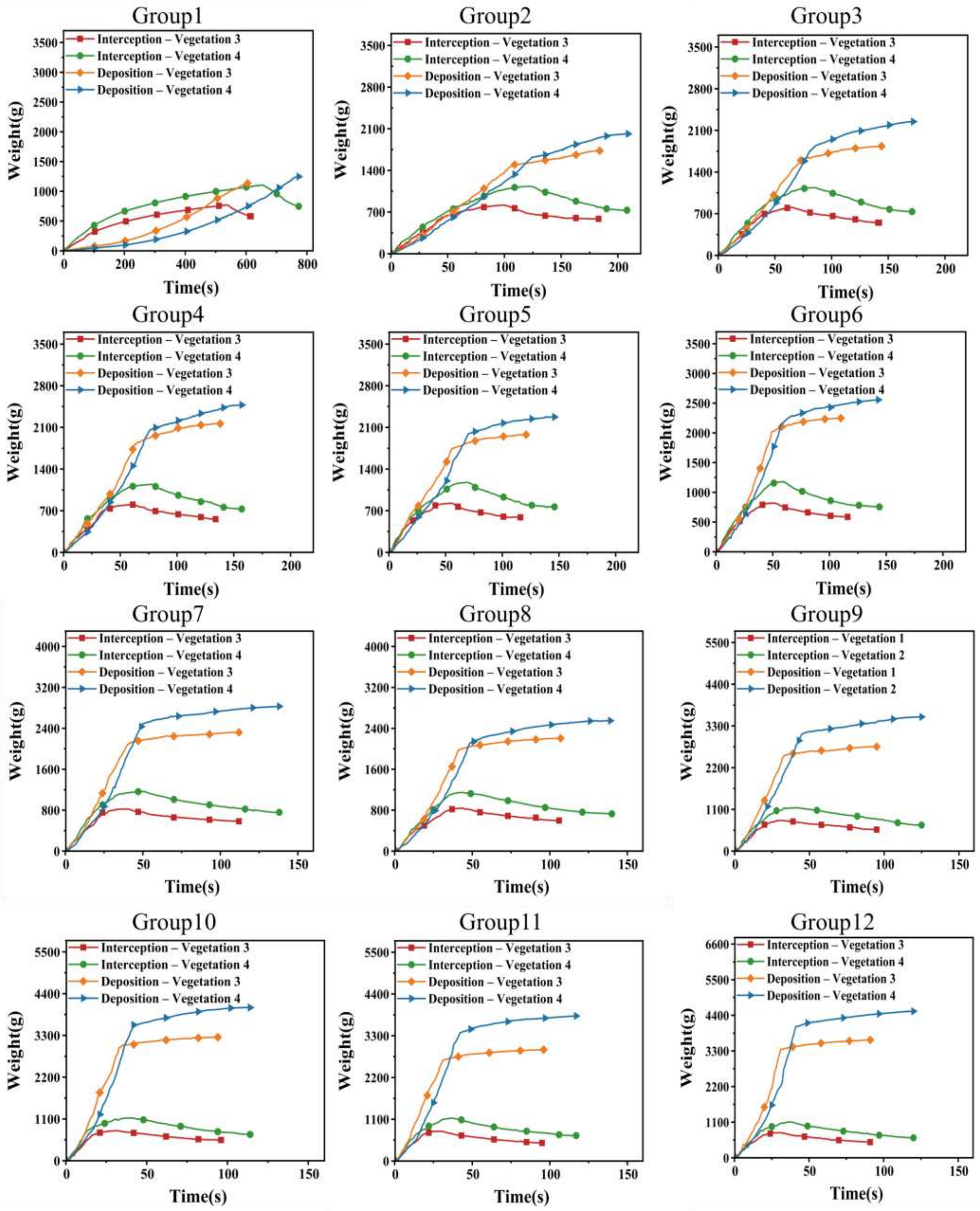

Figure 12 Experimental results for the fire-extinguishing agent canopy interception and ground deposition of *Pinus massoniana* under different drop conditions

To reduce experimental uncertainty and improve data reliability, this study performed three independent replicates under identical spray conditions. The saturated interception, stabilized interception, deposition volume, and spray volume are presented in Table 5. For *Schima superba,* the results were detailed in Tables 5 and 6. The corresponding interception and deposition analyses for *Pinus massoniana* were summarized in Appendix A (Tables 10 and 11).

Table 5 Results for fire-extinguishing agent Canopy Interception and Ground Deposition (Vegetation type 1)

Test group	I_{max} (g)	I_{min} (g)	D (g)	S (g)
1-1	755.3±18.4	549.3±17.4	1125.7±30.9	2012.1±35.2
2-1	742.4±15.2	541.6±11.8	1458.6±28.4	2270.7±20.9
2-2	756.9±12.4	558.7±13.9	1672±35.5	2462.3±25.6
2-3	751.5±10.8	549±12.5	1918.2±40.1	2703.8±28.3
3-1	779.5±15.6	579.7±12.6	1759.5±38.5	2582.9±48.4
3-2	782.8±13.5	577.5±14.2	2085.8±45.6	2938.5±56.8
3-3	784.4±+24.6	584.3±11.3	2185.8±63.5	3050.4±68.1
4-1	762.5±18.6	535.4±9.5	1984.8±48.9	2792.8±62.1
4-2	745.4±20.8	506.9±14.2	2515.9±78.6	3318.8±75.0
4-3	733.4±16.8	489.9±18.1	3098.7±98.6	3942.5±105.3
5-1	728.3±17.2	481.5±17.0	2674.2±84.3	3465.7±85.1
5-2	725.3±19.2	438.0±15.6	3515.2±105.6	4294.5±120.5
Mean value	753.8	531.8	2178.6	2989.3

Table 6 Results for fire-extinguishing agent Canopy Interception and Ground Deposition (Vegetation type 2)

Test group	I_{max} (g)	I_{min} (g)	D (g)	S (g)
1-1	1072.7±21.5	681.3±16.3	913.5±27.5	2282.2±29.2
2-1	1043.6±13.2	685.6±17.4	1478.6±19.6	2614.1±15.6
2-2	1035.1±16.5	677.9±12.5	1891.1±26.4	3051.5±27.6
2-3	1052.4±17.3	686.7±9.8	2103.2±24.5	3228.6±24.3
3-1	1055.6±14.9	693.3±14.6	2045.5±38.6	3214.8±28.0
3-2	1053.2±12.4	690.9±11.5	2221.4±34.7	3367.1±48.5
3-3	1063.2±13.8	714.4±8.9	2489.2±45.7	3665.6±59.9
4-1	1075.7±19.5	707.5±13.0	2188.9±42.6	3315.9±53.2
4-2	1024.6±14.6	645.1±17.6	3188.9±82.6	4315.2±79.3
4-3	1015.4±15.4	621.2±19.3	3627.7±94.8	4765.7±88.6
5-1	1018.1±18.3	625.8±14.2	3468.2±73.2	4578.2±84.5
5-2	1008.3±16.5	600.8±16.1	4108.2±99.8	5274.2±115.4
Mean value	1044.8	672.5	2495.7	3624.3

To verify the experimental data, three independent replicate tests were conducted. The results showed that the standard deviations for all experiments were controlled within 3%, demonstrating strong repeatability and stability. Based on Table 5, Table 6 and Appendix A (Tables 10 and 11), the analysis of mean canopy interception and ground deposition under different spray conditions was presented in Figure 13.

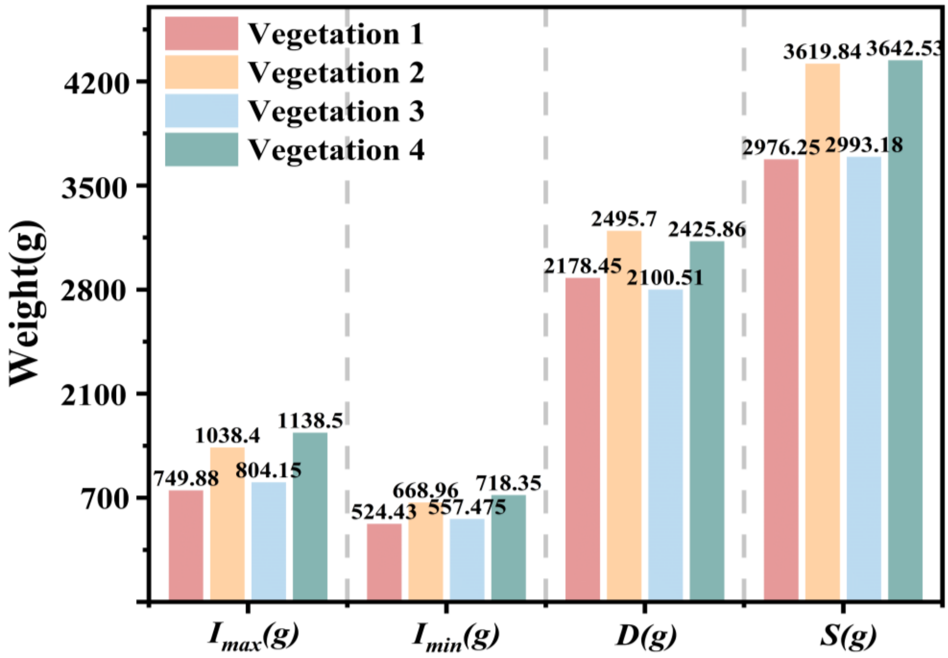

Figure 13 Analysis of the mean canopy interception and ground deposition of fire-extinguishing agent for four vegetation types

Taking Vegetation type 1 as an example and referring to Figures 11 and 13, the droplet dynamics exhibit a three-stage evolution:

(1) *Rapid interception phase*. At the onset of spraying, interception increases sharply while deposition grows more slowly due to the strong retention capacity of the foliage. Within the first 45% of the time to interception saturation, the intercepted amount reaches 64.2% of its saturated value, whereas deposition attains only 35.1% of its saturated amount. This phase is characterized by strong adsorption and droplet capture.

(2) *Steady saturation phase*. As most interception sites on the leaf surface become occupied, marginal interception approaches its physical limit, and the interception growth rate declines. Specifically, the per-unit-time increment in interception accounts for <5% of the applied spray volume, whereas the per-unit-time increment in deposition accounts for >90% of the applied spray volume. This reflects maximized droplet retention on leaves and a system state of near-saturated interception with deposition dominance.

(3) *Lagged dripping phase.* After spraying ceases, droplets begin to slide off leaf surfaces

due to surface tension and gravity. Interception correspondingly decreases, while deposition continues to increase as droplets are transferred to the ground or lower canopy layers.

Regarding the influence of vegetation traits on interception and deposition, this study evaluates canopy interception capacity using the mean saturated interception. In experiments with LAI=1.18, the mean saturated interception of *Pinus massoniana* is 6.9% higher than that of *Schima superba*, while the mean saturated deposition is 3.7% lower. In experiments with LAI=2.10, the mean saturated interception of *Pinus massoniana* is 8.9% higher than that of *Schima superba*, and the mean saturated deposition is 2.9% lower. These results indicate that *Pinus massoniana* exhibits greater saturated interception than *Schima superba*, reflecting a greater canopy interception capacity. Furthermore, LAI has a pronounced effect on droplet interception and deposition.

Regarding the effect of spray parameters on canopy interception, the results showed that spray flow rate has a significant, nonlinear effect on saturated interception. In the low-flow regime (Groups 2-1 and 2-2), saturated interception increases proportionally with the flow rate, whereas in the high-flow regime (Groups 4-2 and 5-1), it becomes inversely related. The underlying mechanism is that, at low flows, interfacial tension and leaf-surface microstructure dominate adhesion. Increasing the spray supply expands the wetted area and enhances retention. However, at excessively high flows, droplet surface adhesion is diminished, leading to coalescence, runoff, and spray bypassing the canopy, which in turn cause wastage and non-uniform deposition.

The above findings demonstrate how vegetation traits and spray parameters jointly influence the interception and deposition of fire-extinguishing agent droplets, revealing phase-dependent droplet behavior across various spray conditions and their close coupling with vegetation traits. Building on the metrics defined in Section 2.2.3, this article further assesses the integrated effects of spray parameters on canopy interception and ground deposition. The mean interception and deposition characteristics for *Schima superba* are reported in Tables 7 and 8, while the corresponding results for *Pinus massoniana* were presented in Appendix A (Tables 12 and 13).

Table 7 Analysis of Mean fire-extinguishing agent Canopy Interception and Ground Deposition Characteristics (Vegetation type 1)

Test group	I_{fall} (*g*)	I_{rate} (%)	D_{rate} (%)	t (*s*)	I_{t} (*g/s*)	D_{t} (*g/s*)
1-1	182.3	41.31%	55.95%	531.8	1.4	1.9
2-1	200.8	31.58%	67.28%	95.0	7.8	16.6
2-2	208.2	30.04%	68.19%	65.4	11.6	27.0
2-3	215.5	27.79%	70.94%	56.7	13.2	33.6
3-1	211.8	30.18%	68.12%	52.2	14.9	32.9
3-2	217.3	26.64%	70.98%	44.5	17.6	46.4
3-3	229.1	25.81%	71.66%	36.2	21.8	61.1
4-1	224.1	27.30%	71.07%	39.1	19.5	49.2
4-2	238.5	22.46%	75.81%	30.2	24.7	80.6
4-3	243.5	18.22%	78.09%	30.7	23.4	100.9
5-1	246.8	20.81%	77.16%	27.8	25.9	92.6
5-2	287.5	16.89%	81.85%	28.2	25.7	126.9
Mean value	225.5	26.59%	71.43%	86.5	17.3	55.8

Table 8 Analysis of Mean fire-extinguishing agent Canopy Interception and Ground Deposition Characteristics (Vegetation type 2)

Test group	I_{fall} (*g*)	I_{rate} (%)	D_{rate} (%)	*t* (*s*)	I_{t} (*g/s*)	D_{t} (*g/s*)
1-1	331.4	50.76%	45.92%	602.8	1.7	1.4
2-1	351	38.20%	60.71%	110.4	9.5	14.7
2-2	357.2	33.92%	63.41%	79.3	13.1	24.7
2-3	365.7	32.16%	65.14%	67.7	15.3	30.6
3-1	362.3	32.84%	63.63%	64.9	16.3	31.6
3-2	367.3	31.58%	65.97%	51.0	20.8	43.7
3-3	358.8	29.28%	67.91%	43.5	24.7	57.7
4-1	368.2	32.34%	65.81%	46.5	23.1	47.5
4-2	379.5	23.74%	73.90%	39.2	26.1	81.6
4-3	394.2	21.31%	76.12%	37.1	27.3	97.6
5-1	390.3	22.24%	75.75%	36.7	27.7	92.5
5-2	407.5	19.37%	78.94%	34.2	29.5	117.8
Mean value	369.5	30.64%	66.94%	101.1	19.6	53.5

Building on the preceding analysis of mean interception and deposition across vegetation types and spray parameters, Figure 14 presents the variations in mean interception rate, deposition rate, and per-unit-time interception and deposition for two representative vegetation types, *Schima superba* and *Pinus massoniana*, under two distinct LAI conditions. The aim is to visually compare the modulatory effects on the distribution characteristics of fire-extinguishing agent droplets.

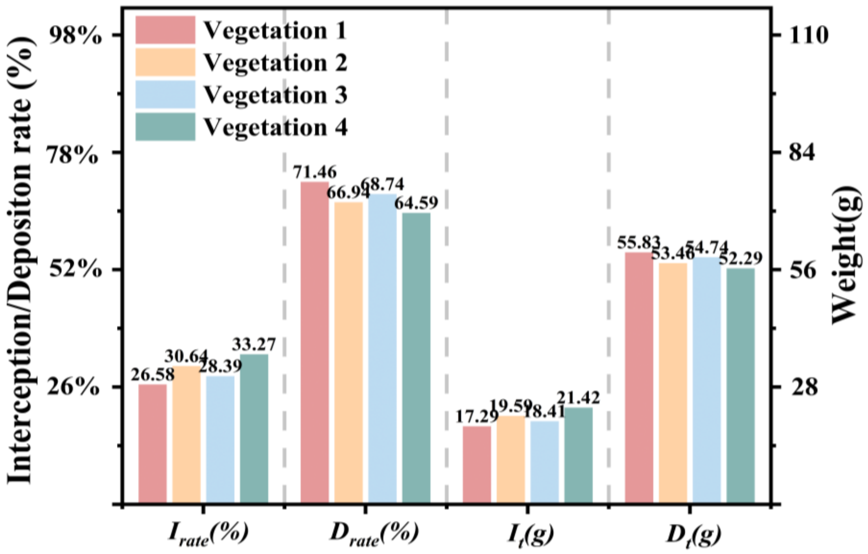

Figure 14 Analysis of Mean Canopy Interception and Ground Deposition Characteristics for four vegetation types

Based on the experimental results, the effectiveness of droplet canopy interception and ground deposition is jointly governed by vegetation type and canopy LAI. From the comparative plot in Figure 14, the mean interception rate, mean deposition rate, time to saturation, and the per-unit-time intercepted and deposited amounts differ significantly across vegetation types. In experiments with LAI=1.2, the conifer Pinus massoniana demonstrates a mean interception rate 1.76% higher than the broadleaf Schima superba, a mean deposition rate 2.54% lower, a per-unit-time mean intercepted amount 1.1g higher, and a per-unit-time mean deposited amount 1.06g lower. In experiments with LAI=2.11, Pinus massoniana exhibits a mean interception rate 2.63% higher than Schima superba, a mean deposition rate 2.35% lower, a per-unit-time mean intercepted amount 1.8g higher, and a per-unit-time mean deposited amount 1.21g lower. These results, together with the analysis of vegetation effects on interception and deposition, indicate that Pinus massoniana possesses a greater canopy interception capacity than Schima superba, and this advantage becomes more pronounced as LAI increases.

Meanwhile, the lagged dripping volume is jointly influenced by leaf hydrophobicity and droplet parameters. In terms of leaf hydrophobicity, as LAI increases, the difference in lagged dripping between Pinus massoniana and Schima superba grows from 9.8% to 11.2%. Combined with the hydrophobicity findings in Section 3.2, this suggests that Pinus massoniana exhibits weaker retention of the fire-extinguishing agent, allowing droplets to slide off leaf surfaces more readily to the ground. In terms of droplet parameters, using Vegetation type 1 as an example, the lagged dripping amount in Group 5-2 was 26.33% higher than in Group 3-1 and 36.59% higher than in Group 1-1. This implies that high flow rates and larger droplet sizes can disturb the adhesion balance and reduce local surface-tension support, thereby promoting downward motion and dripping.

These results demonstrate that vegetation type and canopy structural traits are key determinants of fire-extinguishing agent application efficiency; thus, vegetation-specific operating strategies offer an effective path to improve utilization.

3.4. Relative Importance Analysis of Drop Parameters

This section examines the spray parameters listed in Table 3, which comprise flow rate, velocity, and droplet size as explanatory variables. Using the saturated interception rate and saturated deposition rate measured for *Schima superba* and *Pinus massoniana* under different LAI conditions, a multiple linear regression model (Formu 3-3) was formulated to quantify the relative importance of these three factors in governing the penetration of fire-extinguishing agent droplets through the canopy.

$$y = \beta_0 + \beta_1 Q + \beta_2 V + \beta_3 D_{50} \quad (3\text{-}3)$$

where y denotes the model's dependent variable, β_0 is the intercept, β_1, β_2, and β_3 are the fitted coefficients associated with the flow rate, velocity, and droplet size, respectively.

Because multicollinearity among predictors can undermine the robustness and interpretability of coefficient-based importance metrics, this article first quantifies the interdependence among flow rate, velocity, and droplet size using Variance Inflation Factors (VIFs). Based on the experimental results in Tables 2 and 3, the VIFs for flow rate, velocity, and droplet size are 5.49, 1.27, and 5.21, respectively. According to commonly used thresholds $(VIF > 5)$, notable collinearity is indicated (Kim et al. 2019). The flow rate and droplet size exhibit substantial collinearity under the present conditions.

Building on the above collinearity assessment, this article applied relative importance analysis to decompose the contributions of flow rate, droplet size, and velocity to droplet penetration through the canopy. Unlike unsupervised principal component analysis or simple coefficient-based interpretations, the relative importance approach is invariant to predictor entry order and fairly apportions shared explained variance, thereby yielding more reliable results when predictors exhibit substantial multicollinearity (Das et al. 2025). Accordingly, this study combined the multiple linear regression model with relative-importance decomposition to obtain each predictor's contribution.

$$\eta_j = E_\pi[R^2(S_\pi \bigcup \{j\}) - R^2(S_\pi)] \tag{3-4}$$

where S_π denotes the set of variables that precede variable j within the entry order π; the sum of all equals the model R^2.

By normalizing to percentages, the relative importance share of each predictor was obtained. Meanwhile, to quantify the uncertainty of the LMG method, this study employed a nonparametric bootstrap with replacement at the observation level $(B = 2000)$ and utilized the percentile method to obtain 95% confidence intervals, providing interval estimates and enhancing the robustness of the conclusions.

Based on Tables 2, 3, 5 and 6, this article first established multiple linear regression equations for the saturated interception and deposition of *Schima superba* at LAI=1.1. The fitted linear models were provided in Formulas (3-5) and (3-6).

$$y_I = 0.447561 - 0.015360Q - 0.004966V - 0.000263D_{50} \tag{3-5}$$

$$y_D = 0.522176 + 0.012532Q + 0.005093V + 0.000339D_{50} \tag{3-6}$$

For Formulas (3-5) and (3-6), the linear fit was $R^2 = 0.9762$ and $R^2 = 0.9554$. Based on the relative importance decomposition, the contributions of the three factors to the interception rate (95% CI) were: flow rate 49.44% (45.24%-53.95%); droplet size 39.24% (34.89%-43.81%); and velocity 11.32% (6.67%-17.06%). The contributions to the deposition rate were: flow rate 47.63% (41.79%-53.77%), droplet size 41.48% (35.45%-47.81%), and velocity 10.90% (4.78%-18.65%). As categorized in Table 1, the remaining results were presented in Table 9.

Table 9 Linear Regression Equations and Relative Importance Results

Vegetation	Operating condition	Linear Regression Equations	Relative Importance Results（95% IC）
2	Interception	$y_I = 0.603156 - 0.011460Q - 0.009730V - 0.000212D_{50}$ $R^2 = 0.9768$	Q：**46.36% (42.28%-50.09%)** D_{50}： 39.30% (36.63%-43.77%) V： 14.33% (9.27%-19.84%)
	Deposition	$y_D = 0.332743 + 0.006945Q + 0.011119V + 0.000273D_{50}$ $R^2 = 0.9711$	Q：**44.28% (40.01%-48.63%)** D_{50}： 41.29% (35.84%-46.47%) V： 14.43% (8.86%-20.60%)
3	Interception	$y_I = 0.456895 - 0.016443Q - 0.004505V - 0.000089D_{50}$ $R^2 = 0.9823$	Q：**51.92% (48.52%-55.12%)** D_{50}： 38.80% (35.11%-42.55%) V： 9.28% (5.82%-13.83%)
	Deposition	$y_I = 0.462254 + 0.010331Q + 0.006956V + 0.000157D_{50}$ $R^2 = 0.9708$	Q：**47.48% (43.13%-51.70%)** D_{50}： 39.97% (35.06%-44.94%) V： 12.54% (7.49%-18.81%)
4	Interception	$y_I = 0.658198 - 0.011873Q - 0.010491V - 0.000235D_{50}$ $R^2 = 0.9777$	Q：**46.24% (42.27%-50.25%)** D_{50}： 39.77% (35.05%-44.26%) V： 13.99% (9.02%-19.55%)
	Deposition	$y_I = 0.316966 + 0.006958Q + 0.011193V + 0.000264D_{50}$ $R^2 = 0.9711$	Q：**44.12% (39.80%-48.44%)** D_{50}： 40.53% (35.25%-45.70%) V： 15.34% (9.55%-21.78%)

Based on the above analysis, the results of key spray parameters reveal a robust and consistent ranking across various vegetation conditions. Specifically, for interception, the average relative contributions of the three variables are approximately: flow rate 49.28%, droplet size 40.77%, and velocity 10.82%. For deposition, they are: flow rate 46.95%, droplet size 41.92%, and velocity 11.13%. Accordingly, a stable ordering is established: flow rate>droplet size>velocity. The signs of the coefficients indicate that for all vegetation types, increases in flow rate, velocity, and droplet size are associated with a decrease in the interception and an increase in the saturated deposition. This suggests that these factors enhance the ability of droplets to penetrate the canopy and reach the ground. Therefore, in operational practice, adjusting flow rate should be prioritized as the primary control lever, droplet size as a secondary control, and velocity for fine calibration, subject to drift constraints.

3.5. Aerial Application Strategy Recommendations of fire-extinguishing agent

In firebreak construction operations, targets are classified into ground fire and crown fire, each with distinct tactical objectives. The former prioritizes the formation of a continuous, sufficiently thick ground line, emphasizing ground load, deposit thickness, line width, and coverage uniformity. The latter focuses on increasing canopy fire-extinguishing agent interception and band continuity to sever the spatial continuity of crown fuels and suppress outward spread. Therefore, in practical spray operations, a hierarchical parameter control strategy should be followed. First, use flow rate as the primary control lever, then adjust droplet size as a secondary lever to balance penetration and drift, and finally, use velocity for fine calibration. At the same time, strategies should be tailored to local vegetation characteristics and specific operational objectives.

When ground deposition is the primary objective, hovering or low-speed straight flight paths are recommended to extend the interaction time with the canopy and increase the effective delivery per unit time. Flight lines should adopt slightly reduced spacing with appropriate overlap, combined with low-to-moderate release heights and upwind or slight downwind approaches at small angles to the wind to reduce crosswind shear and long-range drift. In terms of equipment, priority should be given to tanks or nozzles with larger orifices to achieve higher instantaneous flux and improve droplet penetration into the canopy. For canopies with higher cover or conifer dominance, a top-down, layered application supplemented by repeated flight lines is recommended to offset losses from strong interception and intra-canopy redistribution, thereby forming a continuous, robust ground-deposition line.

Conversely, when canopy interception is the main objective, medium-speed passes should be used to increase the fireline formation rate and boundary closure efficiency. Flight-line organization should emphasize continuous parallel bands with moderate spacing, and the areal flux should be maintained at a moderate level to improve canopy interception and band continuity. In coniferous or high-cover settings, short-interval repeats on the same track or alternating re-sweeps of adjacent bands should be employed to mitigate the effects of lagged dripping and to increase canopy retention.

4. Conclusions

This study elucidated, at the canopy penetration stage, how vegetation type and droplet properties govern the canopy interception, ground deposition, and lagged dripping. The results show that, in terms of vegetation traits, *Pinus massoniana* exhibits stronger canopy interception and lagged-dripping capacities than the broadleaf *Schima superba*. This advantage becomes more pronounced with increasing LAI. A relative importance analysis of spray parameters revealed a robust ranking of influence: *flow rate>droplet size>velocity.* An analysis of the regression coefficients further indicates that, when other variables are held constant, increases in flow rate, droplet size, and velocity make fire-extinguishing agent droplets more likely to penetrate the canopy and deposit on the ground. Based on these findings, a hierarchical operational strategy is proposed: use flow rate as the primary control, adjust droplet size as a secondary lever to balance penetration and drift, and employ velocity for fine calibration, thereby optimizing the efficiency of firebreak construction with fire-extinguishing agent.

However, this study has the following limitations. In terms of materials selection, the experiment was conducted at the potted scale, which cannot adequately capture the heterogeneity of natural forests. In experimental design, the nozzle-based simulation of the canopy penetration stage did not incorporate aircraft-induced flow, crosswinds, turbulence, or release height, introducing uncertainty when extrapolating to actual aerial application conditions. Future work should extend to natural stands to characterize canopy properties at a realistic vegetation scale and integrate wind tunnel testing and UAV rotor downwash platforms to refine boundary conditions and uncertainty reporting.

Reference

Álvarez, C., Correa, N., Valenzuela, F., et. al, 2025. Bench-scale flammability testing to optimize the effectiveness of fire retardant treatment of wildland fuels. Fire Safety Journal 157,104509. https://doi.org/10.1016/j.firesaf.2025.104509.

Calogine, D., Rimbert, N., Séro-Guillaume, O.,2007. Modelling of the deposition of retardant in a tree crown during fire fighting. Environmental Modelling & Software. 22, 1654-1666. https://doi.org/10.1016/j.envsoft.2007.01.003.

Chen, D., Wang, M., Si, L., Zhao, F., Shu, L., 2023. Study on Tree Species Selection of Biological Fire Barrier in Sichuan Province. Terrestrial Ecosystem and Conservation. 3(2), 56-68. CNKI:SUN:LDST.0.2023-02-007.

Cui, X., Alam, M. A., Perry, G. L. W., Paterson, A. M., et al., 2019. Green firebreaks as a management tool for wildfires: Lessons from China. Journal of Environmental Management. 233, 329-336. https://doi.org/10.1016/j.jenvman.2018.12.043.

Czyż, Z., Karpiński, P., Skiba, K., Bartkowski, S., 2023. Numerical calculations of water drop using a firefighting aircraft. Applied Computer Science. 19(3), 47-63. https://doi.org/10.35784/acs-2023-24.

Das, P., Afroz, F., Rahman, M.H., et, al.,2025. Comparison of two measures of relative importance of predictors in logistic regression. Discov Appl Sci. 7 , 352. https://doi.org/10.1007/s42452-025-06818-4.

Dominique L., 2024.Fluid Dynamics of Airtanker Firefighting, Annual Review of Fluid Mechanics. 56, 577-603, https://doi.org/10.1146/annurev-fluid-121021-041642.

Erinin, M.A., Néel, B., Mazzatenta, M.T., et, al.,2023. Comparison between shadow imaging and inline holography for measuring droplet size distributions. Experimental Fluids. 64, 96. https://doi.org/10.1007/s00348-023-03633-8.

Fischer, D.G., Vieira, S.T., Jayakaran, A.D., 2023.Distinct rainfall interception profiles among four common Pacific Northwest tree species. Forests. 14(1) ,144. https://doi.org/10.3390/f14010144.

Gaikwad, H. B., Kumar,A. 2024. Flammability of tropical forest litter with and without fire retardant. Fire Safety Journal. 144, 104106. https://doi.org/10.1016/j.firesaf.2024.104106.

Ingalsbee, T. 2005.Fuelbreaks for Wildland Fire Management: A Moat or a Drawbridge for Ecosystem Fire Restoration? fire ecol.1, 85-99. https://doi.org/10.4996/fireecology.0101085.

Ito, T., Kato, Goda, H. Y., Tagawa, S., Negishi, E., 2010.Water-dropping aerodynamics for firefighting amphibian. Congress of the International Council of the Aeronautical Sciences, Japan Aerospace Exploration Agency (JAXA); ShinMaywa Industries Ltd.; Japan Aircraft Development Corporation (JADC) .https://api.semanticscholar.org/CorpusID:201049077.

Kim, J.H. ,2019. Multicollinearity and misleading statistical results. Korean J Anesthesiol. 72(6), 558-569. 10.4097/kja.19087. Epub 2019 Jul 15.

Kuznetsov, G.V., Islamova, A.G., Orlova, E.G., Strizhak, P.A., Feoktistov, D.V., 2021. Physicochemical features of the effect of special water-based fire retardants on forest materials. Fire Safety Journal. 123, 103371. https://doi.org/10.1016/j.firesaf.2021.103371.

Lattimer, B.Y., Huang, X., Delichatsios, M.A. et al. Use of Unmanned Aerial Systems in Outdoor Firefighting. Fire Technology. 59, 2961-2988 2023. https://doi.org/10.1007/s10694-023-01437-0.

Loudermilk, E.L., O'Brien, J.J., Goodrick, S.L.et al. 2022. Vegetation's influence on fire behavior goes beyond just being fuel. fire ecol. 18, 9. https://doi.org/10.1186/s42408-022-00132-9.

Liu, A., Delichatsios, M., Levendis, Y., 2022. On the trajectory and reach of fire-suppressant liquid nitrogen droplets released from a spray nozzle. Process Safety and Environmental Protection. 161,273-284. https://doi.org/10.1016/j.psep.2022.03.046.

Liu, J., Zhao, L., Wang, Q., Jiang, N., Liu, J.,2024. PIV experimental analysis of the escape phenomenon of air spraying jet in factories. Journal of Building Engineering. 82, 108384. https://doi.org/10.1016/j.jobe.2023.108384.

Lu, J.; Zhou, T.; Wu, C.; Ou, Y., 2023. Dropping Fire Retardants by Helicopter and Its Application to Wildfire Prevention near Electrical Transmission Lines. Fire. 6, 176, https://doi.org/10.3390/fire6050176.

Ma, J., Liu, K., Dong, X., Chen, C., Qiu, B., Zhang, S., 2022.Effects of Leaf Surface

Roughness and Contact Angle on In Vivo Measurement of Droplet Retention. Agronomy. 12, 2228. https://doi.org/10.3390/agronomy12092228.

Nasiri, M., Amini, G., Moreau, C., Dolatabadi, A.,2021. Hollow droplet impact on a solid surface. International Journal of Multiphase Flow. 143, 103740. https://doi.org/10.1016/j.ijmultiphaseflow.2021.103740.

Papakonstantinou, C. A., Chen, H., Amirfazli, A., 2022. New ellipse-fitting method for contact angle measurement. Surface Innovations. 10(6), 387-394. https://doi.org/10.1680/jsuin.21.00028.

Shan, C., Xue, C., Zhang, L., Song, C. R. Kaousar, G. Wang, Y. Lan, 2024. Effects of different spray parameters of plant protection UAV on the deposition characteristics of droplets in apple trees. Crop Protection. 184 ,106835. https://doi.org/10.1016/j.cropro.2024.106835.

Shrigondekar, H., Chowdhury, A. & Prabhu, S.V, 2021. Performance by Various Water Mist Nozzles in Extinguishing Liquid Pool Fires. Fire Technology Fire Technology. 57, 2553-2581. https://doi.org/10.1007/s10694-021-01130-0.

Silva, J.E., da Silva, W.H.B., Ferraz, M.A.J., et, al., 2024. impact of spray volume and flight speed on the efficiency of drone applications in coffee plants of different ages. Smart Agricultural Technology. 9, 100694. https://doi.org/10.1016/j.atech.2024.100694.

Struminska, A., Filippone, A.,2024. Flight performance analysis of aerial firefighting. The Aeronautical Journal. 128,1895-1923. https://doi.org/ 10.1017/aer.2024.29.

Tang, Q., Zhang, R., Chen, L., Deng, W., Xu, M., Xu, G., Li, L., Hewitt, A., 2020. Numerical simulation of the downwash flow field and droplet movement from an unmanned helicopter for crop spraying, Computers and Electronics in Agriculture. 174, 105468. https://doi.org/10.1016/j.compag.2020.105468.

Tezcan, T. , 2025. Forest fire management and fire suppression strategies: a systematic literature review. Nat Hazards. 121, 10485-10515. https://doi.org/10.1007/s11069-025-07227-x.

Tian, Y., 2019. Research on numerical simulation method of large firefighting aircraft water-dropping process. Flight Dynamics. 037(003), 83-86. 10.13645/j.cnki.f.d.20190122.001.

Wang, L., Ni, S., Wang, H., Sun, Y., Fu, S., et, al., 2023.Influence of wettability alteration on water-blocking effect and gas desorption of coal. Process Safety and Environmental Protection. 180, 361-374. https://doi.org/10.1016/j.psep.2023.10.003.

Wang, S., Nuyttens, D., Lu, D., et. al, 2023.Airflow characteristics of a spray UAV and its effect on spray droplet transportation. Engenharia Agrícola. 43(6), 10.1590. https://doi.org/10.1590/1809-4430-Eng.Agric.v43n6e20230041/2023.

Wang, Y., Cheng, J., Zhang, J., Kan, X., 2018. Effects of Undergrowth Typical Vegetation on Water Interception in the Simian Mountain of Chongqing. Journal of Soil and Water Conservation. 32(4),81-87. 10.13870/j.cnki.stbcxb.2018.04.013.

Widmann, J.F., Sheppard, D.T. , Lueptow, R.M. 2001. Non-Intrusive Measurements in Fire Sprinkler Sprays.Fire Technology. 37, 297-315. https://doi.org/10.1023/A:1012727614590.

Wolter, P.T., Olbrich, J.J., Johnson, P.J. 2021. Modeling sub-boreal forest canopy bulk density in Minnesota, USA, using synthetic aperture radar and optical satellite sensor data. Fire ecol. 17, 26. https://doi.org/10.1186/s42408-021-00112-5.

Xu, L., Yang, Z., Huang, Z., et, al., 2023.Effects of flight parameters for plant protection UAV on droplets deposition rate based on a 3D simulation approach. International Journal of Agricultural and Biological Engineering. 16(1), 66-72. 10.25165/j.ijabe.20231601.6581.

Yang, C., Wallace, R.J., Huang, C, 2024. A review and bibliometric analysis of unmanned aerial system (UAS) noise studies between 2015 and 2024. Acoustics. 6,997-1020. https://doi.org/10.3390/acoustics6040055.

Yang, J., He, Z., Lin, P., Du, J., Shi, D., Bai, M., 2024.Uncertainty of canopy interception modeling in high-altitude Picea crassifolia forests of semi-arid regions. Agricultural and Forest Meteorology. 356,110190. https://doi.org/10.1016/j.agrformet.2024.110190.

Yao, W., Lan, Y., Hoffmann, Li, C. J., Guo, S., Zhang, H., Wang, J., 2020. Droplet size distribution characteristics of aerial nozzles by Bell206L4 helicopter under medium and low airflow velocity wind tunnel conditions and field verification test. Applied Sciences. 10, 2179. https://doi.org/10.3390/app10062179.

Yi, Q., Hou, S., Dou, X., Gao, Y., Li, Z., Liu, Y., 2025.Analysis and simulation of interception characteristics of broad-leaved forest canopy based on parameter optimization: Dianchi basin case. Ecological Indicators. 173, 113352.https://doi.org/10.1016/j.ecolind.2025.113352.

Zhang, J., Chen, Q., Liu, J., Wang, Y., 2024. Experiments and CFD simulation of downwash airflow and fog distribution discharged from a single-rotor UAV fitted with a pulse-jet thermal fogging machine. Biosystems Engineering. 240, 142-151. https://doi.org/10.1016/j.biosystemseng.2024.03.007.

Zhao, J., Wang, Y., Meng, Z., Du, H., Ma L., et al., 2023. Spatiotemporal patterns of fire-driven forest mortality in China. Forest Ecology and Management. 529, 120678. https://doi.org/10.1016/j.foreco.2022.120678.

Zhou, X., Zhou, Y., Wang, Y., Bai, Y., Feng, J., 2025.The redistribution of rainfall in mixed coniferous–broadleaf forests: The combined effect of rainfall characteristics and stand structure. Trees, Forests and People. 22, 100989. https://doi.org/10.1016/j.tfp.2025.100989.

Zwertvaegher, I.K., Verhaeghe, M., Brusselman, E., Verboven, P., Lebeau, F., Massinon, M., Nicolaï, B.M., Nuyttens, D., 2014.The Impact and retention of spray droplets on a horizontal hydrophobic surface. Biosystems Engineering. 126, 82-91. https://doi.org/10.1016/j.biosystemseng.2014.07.013.

Appendix A. Analysis of Fire-extinguishing Agent Canopy Interception and Ground Deposition Results

Table 10 Results for fire-extinguishing agent Canopy Interception and Ground Deposition (Vegetation type 3)

Test group	I_{max} (g)	I_{min} (g)	D (g)	S (g)
1-1	771.7±14.6	589±16.6	915.2±27.5	1715.1±18.4
2-1	808.3±12.8	579.5±13.2	1497.2±25.7	2351.5±23.5
2-2	809.5±15.6	577.6±11.5	1589.2±35.6	2451.2±34.8
2-3	815.1±11.5	575.3±12.4	1852.8±30.5	2725.1±30.4
3-1	817.5±14.4	582.4±12.7	1750.2±37.6	2648.6±42.3
3-2	821.9±13.2	583.2±16.1	2015.7±38.7	2964.5±51.9
3-3	828.2±17.3	581.1±13.4	2081.7±54.9	3012.3±64.7
4-1	822.7±17.5	575.9±13.5	1972.4±40.2	2883.9±55.4
4-2	810.0±14.8	552.5±18.7	2525.3±69.7	3435.3±72.5
4-3	780.2±16.6	500.7±20.9	2982.1±85.1	3914.6±89.4
5-1	789.6±15.9	516.1±17.2	2675.6±74.3	3598.7±82.3
5-2	775.1±18.2	476.4±13.6	3345.7±102.6	4216.5±106.6
Mean value	804.15	557.5	2100.3	3014.9

Table 11 Results for fire-extinguishing agent Canopy Interception and Ground Deposition (Vegetation type 4)

Test group	I_{max} (g)	I_{min} (g)	D (g)	S (g)
1-1	1107.2±8.9	747.7±11.9	885.3±28.4	2094.1±14.8
2-1	1124.5±14.3	725.7±13.3	1615.6±29.6	2785.4±25.1
2-2	1138.1±11.5	735.2±15.1	1845.9±24.7	3015.7±20.4
2-3	1142.5±17.0	729.7±17.5	2065.2±35.6	3275.2±22.4
3-1	1174.7±15.8	765.0±8.4	1992.7±33.5	3204.2±31.4
3-2	1177.7±12.9	756.2±16.4	2135.2±47.5	3337.8±42.6
3-3	1163.4±14.6	744.6±14.7	2385.1±37.5	3635.1±35.1
4-1	1147.5±18.2	730.3±18.7	2122.1±42.6	3295.4±34.2
4-2	1141.8±14.1	706.1±14.5	3082.1±76.5	4297.2±64.3
4-3	1115.6±16.2	663.2±16.4	3557.7±81.5	4772.4±74.5
5-1	1121.4±18.4	675.9±19.0	3368.2±71.4	4673±70.2
5-2	1108.3±14.9	640.6±17.1	4055.2±94.5	5304.5±92.5
Mean value	1146.6	723.25	2401.1	3642.5

Table 12 Analysis of Mean fire-extinguishing agent Canopy Interception and Ground Deposition Characteristics (Vegetation type 3)

Test group	I_{fall} (g)	I_{rate} (%)	D_{rate} (%)	t (s)	I_{t} (g/s)	D_{t} (g/s)
1-1	189.7	44.46%	54.45%	520.0	1.5	1.7
2-1	228.8	34.37%	63.67%	95.0	8.5	15.8
2-2	231.9	33.02%	64.83%	63.7	12.7	24.3
2-3	239.8	29.91%	67.99%	57.2	14.3	32.7
3-1	235.1	30.87%	66.08%	53.5	15.3	33.5
3-2	238.7	27.72%	67.99%	44.9	18.3	45.3
3-3	247.1	27.49%	69.11%	35.7	23.2	57.6
4-1	246.8	28.53%	68.39%	40.3	20.4	50.5
4-2	257.5	23.58%	73.51%	31.2	25.9	83.7
4-3	279.5	19.93%	76.18%	30.5	25.6	97.1
5-1	273.5	21.94%	74.35%	28.9	27.4	96.2
5-2	298.7	18.38%	79.35%	27.7	28.0	118.5
Mean value	247.3	28.39%	68.74%	85.7	18.4	54.7

Table 13 Analysis of Mean fire-extinguishing agent Canopy Interception and Ground Deposition Characteristics (Vegetation type 4)

Test group	I_{fall} (g)	I_{rate} (%)	D_{rate} (%)	t (s)	I_{t} (g/s)	D_{t} (g/s)
1-1	359.5	52.87%	42.28%	634.6	1.7	1.5
2-1	398.8	40.37%	58.00%	112.5	10.0	14.6
2-2	402.9	37.74%	61.21%	78.3	14.5	23.3
2-3	412.8	34.88%	63.06%	68.7	16.6	30.5
3-1	409.8	36.66%	62.19%	64.7	18.1	30.7
3-2	421.5	35.07%	63.59%	50.9	23.1	41.9
3-3	418.8	32.00%	65.61%	43.1	27.0	54.9
4-1	417.2	34.82%	64.40%	46.1	24.9	45.6
4-2	435.7	26.57%	71.72%	39.1	29.2	78.6
4-3	452.4	23.38%	74.55%	37.2	30.0	95.8
5-1	445.5	24.00%	72.07%	37.5	29.9	91.7
5-2	467.7	20.89%	76.45%	34.9	31.8	118.6
Mean value	420.2	33.27%	64.59%	104.0	21.4	52.3